Supporting Information for

Multistep Crystallization Process Involving Sequential Formations of Density Fluctuations, "Intermediate Structures", and Lamellar Crystallites: Poly(3-hydroxybutyrate) as Investigated by Time-Resolved Synchrotron SAXS and WAXD

Longhai Guo[1], Nicolas Spegazzini[1], Harumi Sato[1*], Takeji Hashimoto[1,2], Hiroyasu Masunaga[3], Sono Sasaki[3], Masaki Takata[3], Yukihiro Ozaki[1*]

1. *Department of Chemistry, School of Science and Technology and Research Center of Environmental Friendly Polymer, Kwansei-Gakuin University, Gakuen 2-1, Sanda, Hyogo 669-1545, Japan*

2. *Professor Emeritus, Kyoto University, Kyoto 606-8501, Japan, and Honorary Chair Professor, National Tsing Hua Unversity, Hsinchu 30013, Taiwan*

3. *Japan Synchrotron Radiation Research Institute, 1-1-1, Kouto, Sayo-cho, Sayo-gun, Hyogo 679-5198 Japan*

4. *Kyoto Institute of Technology, Matsugasaki, Sakyo-ku, Kyoto 606-8585 Japan*

To whom all correspondence should be addressed.

E-mail: ozaki@kwansei.ac.jp and hsato@kwansei.ac.jp.

This PDF file includes:

Supporting Information 1: One-dimensional Correlation Function Analysis;

Supporting Information 2: MCR-ALS and EFA Algorithm and Their Results;

Supporting Information 3: Avrami Plots on $X_{C,app}(t)$ and $X_{crys}(t)$;

Supporting Information 4: Heterospectral and Homospectral 2D-COS Analyses with tr-SAXS Profiles

and Their Results

Supporting Information 1: One-dimensional Correlation Function Analysis

The characteristic parameters such as the average thickness amorphous layer [$l_a(t)$], the average thickness of the mesomorphic layers having the intermediate structures and/or the lamellar crystallites [$l_c(t)$], and the average long period [$L(t)$] were estimated from the one-dimensional correlation function, $\gamma(z;t)$, according to the method proposed by Strobl and Schneider[1], as demonstrated in Figure S1-1. The average long period is determined by the value z at the first maximum of $\gamma(z;t)$. The average thickness of one of the two layers (l_1) is given by the intersection point between the straight line in the self-correlation part (straight line a) and base line drawn through the first minimum of $\gamma(z;t)$ parallel to the z-axis (straight line b). The average thickness of the other layer is then obtained from $l_2 = L - l_1$. The assignment of l_1 and l_2 are done with respect to information on the local volume fractions of the two layers $X_i = l_i/L$ (i =1 or 2) obtained from other experiments or some physical in sights. As shown in Figure S1-2, $X_1(t)$ and $X_2(t)$ decreases and increase as a function of time, respectively. During the isothermal crystallization process, the local apparent crystallinity should increase with time, and hence l_1 should be attributed to the average thickness of the mesomorphic layers and/or the lamellar crystallites [$l_c(t)$], and l_2 should be attributed to the average thickness of the amorphous layers [$l_a(t)$].
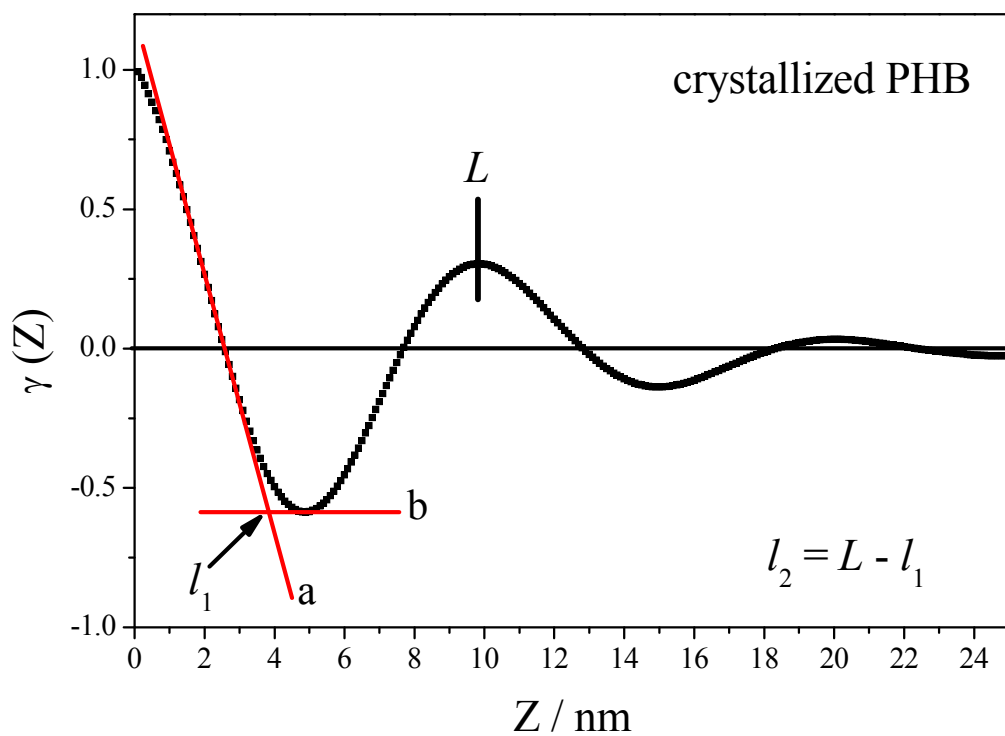
Figure S1-1: The analysis of one-dimensional correlation function obtained at t = 200 s: L = 9.8 nm, l_1 = 3.8 nm, and l_2 = 6.0 nm.
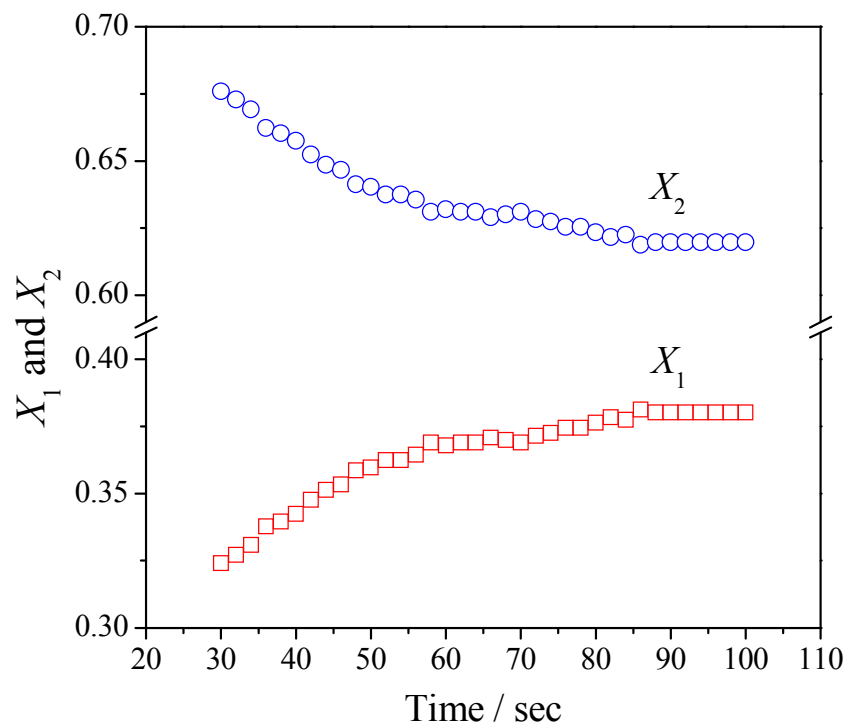

Figure S1-2: Volume fractions $X_i = l_i/L$ of the layer i (i = 1, 2) as a function of time.

Supporting Information 2: MCR-ALS and EFA Algorithm and Their Results

Multivariate Curve Resolution (MCR) designs a group of techniques which intend to recover the pure response profiles of the chemical constituents or species of an unresolved mixture when no apriori information is available about the nature and composition of the mixture. The basic assumption of this method in this manuscript is that the observed WAXD profiles of "non-amorphous phase" can be decomposed into the sum of individual elemental profiles, which are turned out to be the intermediate structures having mesomorphic orders and the lamellar crystallites, respectively. Among MCR methods, the one based on alternating least squares (MCR-ALS) has been wildly and popularly applied to various systems, which was first introduced by Karjlainen[2] and later extended by Tauler[3-6]. By using MCR-ALS analysis, we extracted the elemental WAXD profiles from the intermediate structures and the lamellar crystallites as shown by the red broken lines and blue solid lines, respectively, on the left side of Figure 10 in the text, from the time-resolved WAXD profiles corrected for the amorphous halo, $I_{\mathrm{WAXD}}^{\mathrm{c,app}}(q;t)$

The primary purpose of the MCR-ALS analysis is to transform the experimental data matrix $\mathbf{D} = (D_{i,j})$, where $D_{i,j} = I_{\mathrm{WAXD}}^{\mathrm{c,app}}(q_j;t_i)$ with $i = 1$ to n and $j = 1$ to m, into the matrices $\mathbf{C}$ and $\mathbf{S}^{\mathrm{T}}$, which have a real physical significance, according to the following equation:

$$\mathbf{D} = \mathbf{C}\mathbf{S}^{\mathrm{T}} + \mathbf{E} \tag{S2.1}$$

The matrix $\mathbf{C}$, which is given by $\mathbf{C} = (C_{i,k})$ where $C_{i,k} = W_k(t_i)$ with $i = 1$ to n and $k = 1$ to l (l is turned out to be 2 in this work), has the column vectors corresponding to the weight fractions of the intermediate structures having mesomorphic orders and the lamellar crystallites as a function of time, and the matrix $\mathbf{S}^{\mathrm{T}}$, which is given by $\mathbf{S}^{\mathrm{T}} = (\mathbf{S}^{\mathrm{T}}_{k,j})$ where $\mathbf{S}^{\mathrm{T}}_{k,j} = I_k(q_j)$ with $k = 1$ to l and $j = 1$ to m, has the row vectors corresponding to the elemental profiles as a function of q. Due to the unavoidable experimental uncertainties (noise etc.), this matrix decomposition of MCR-ALS analysis is not perfect,

and the differences between the experimental WAXD profiles and the reconstructed WAXD profiles give rise to matrix **E** of residuals.

The general scheme of the MCR-ALS analysis for obtaining the elemental WAXD profiles from the intermediate structures $I_{inter}(q)$ and the lamellar crystallites $I_{crys}(q)$ and their weight fractions $W_{inter}(t)$ and $W_{crys}(t)$ from $I_{WAXD}^{c,app}(q;t)$ is shown in Figure S2-1 in conjunction with Figure 10 in the text. In the context of this algorithm, the number of components l in $I_k(q_j)$ and $W_k(t_i)$ with $k = 1$ to l (l turns out to be 2 in this work) for the MCR-ALS analysis has to be determined first, which can be carried out by the evolving factor analysis (EFA) (see Figure S2-1).[7] During the calculation of EFA, we started with the matrix $\mathbf{D}_p = (D_{i,j})$ with $i = 1$ to p (p is the starting point and equals to 2 diffraction profiles) and $j = 1$ to m, which was evaluated by using the singular value decomposition algorithm[8], as given by

$$\mathbf{D}_p = \mathbf{U}_p \mathbf{S}_p \mathbf{V}^{\mathrm{T}}_p \tag{S2.2}$$

where $\mathbf{U}_p$, $\mathbf{S}_p$, $\mathbf{V}^{\mathrm{T}}_p$ are respectively the left singular matrix, singular values (root square of eigenvalues) matrix, and right singular matrix of $\mathbf{D}_p$. Sequentially, the matrix $\mathbf{D}_{p+q} = (D_{i,j})$ with $i = 1$ to $p + q$, $j = 1$ to m, and $q = 1$ was evaluated as given by

$$\mathbf{D}_{p+q} = \mathbf{U}_{p+q}\, \mathbf{S}_{p+q}\, \mathbf{V}^{\mathrm{T}}_{p+q} \tag{S2.3}$$

where $\mathbf{U}_{p+q}$, $\mathbf{S}_{p+q}$, $\mathbf{V}^{\mathrm{T}}_{p+q}$ are respectively the left singular matrix, singular values (root square of eigenvalues) matrix, and right singular matrix of $\mathbf{D}_{p+q}$. This evaluation was continuously carried out for the matrix $\mathbf{D}_{p+q} = (D_{i,j})$ with $i = 1$ to $p + q$ and $j = 1$ to m until $p + q = n$ (n equals to the total number of diffraction profiles) as matrix $\mathbf{D}_n$ equals to the experimental data matrix **D**. Meanwhile, the eigenvalues were calculated in both directions (forward and backward, respectively).[9] The forward analysis provides information about the appearance of the different components along the experimental time, whereas the backward analysis provides information about their disappearance. The results of EFA forward and

backward analyses on the experimental data matrix of the tr-WAXD profiles $I_{\text{WAXD}}^{\text{c,app}}(q;t)$ in the q regions of 9 – 10.2 nm^{-1} are shown in Figure S2-2, in which log of the eigenvalues of the experimental data matrix vs time are plotted. The onset of the evolution of the new components in the forwards direction at the evolution times 16 and 32 s is very clearly indicated by the rise of the two new eigenvalues out of the noise level. Meanwhile, the plots of the eigenvalues in the backwards direction also show that there are two significant components in the tr-WAXD profiles. Moreover, the results of EFA forward and backward analyses on the experimental data matrix of the tr-WAXD profiles $I_{\text{WAXD}}^{\text{c,app}}(q;t)$ in the q regions of 11.4 – 12.4 nm^{-1}, and 13 – 17 nm^{-1} are shown in Figure S2-3, and S2-4, respectively, which also indicate that there are two significant components in the tr-WAXD profiles. Through the analyses described in the text, these two components were determined as the intermediate structures and the lamellar crystallites, respectively. Once the eigenvalues are calculated for the experimental data matrix of tr-WAXD profiles $I_{\text{WAXD}}^{\text{c,app}}(q;t)$, an "abstract evolutional plot" of the two components can be deduced from the eigenvalue as the initial estimates of $\mathbf{C}$ matrix as shown in Figure S2-1 for the following MCR-ALS analysis.

Two components were used as an initial estimates of $\mathbf{C}$ matrix in the alternating least squares optimization process[2-6] by MCR-ALS analysis through the following steps: (a) an estimation is performed from the linear equation by least squares $\mathbf{S}^{\text{T}} = \mathbf{C}^{*}\mathbf{D}$, where $\mathbf{C}^{*}$ is the pseudoinverse of matrix $\mathbf{C}$; (b) a new estimation of the matrix $\mathbf{C}$ is obtained by least squares using equation $\mathbf{C} = \mathbf{D}(\mathbf{S}^{\text{T}})^{*}$, where $(\mathbf{S}^{\text{T}})^{*}$ now is the pseudoinverse of matrix $\mathbf{S}^{\text{T}}$; (c) steps (a) and (b) are repeated until the data $\mathbf{D}$ is well explained within the experimental error matrix $\mathbf{E}$. The MCR-ALS analysis in the q region of 9 – 10.2 nm^{-1} yields the normalized elemental WAXD profiles of the intermediate structures and the lamella crystallites [designated as $I_{\text{inter}}(q)$ and $I_{\text{crys}}(q)$ on the left side of Figure 10 (a) in the text, respectively]

and the time evolution of their weight fraction [designated as $W_{inter}(t)$ and $W_{crys}(t)$ on the right side of Figure 10 (a) in the text, respectively]. The experimental time-resolved WAXD profiles and the residual matrix **E** were also shown in Figure S2-5 (a) and (b), respectively. Meanwhile, the corresponding results of the experimental time-resolved WAXD profiles and the residual matrices **E** through the MCR-ALS analyses in the q regions of $11.4 - 12.4$ nm^{-1} and $13 - 17$ nm^{-1} are shown in Figure S2-6 and S2-7, respectively. It can be found that, compared with the observed WAXD diffraction profiles, the residual matrix is very weak, and hence it is negligible for the correct analysis.
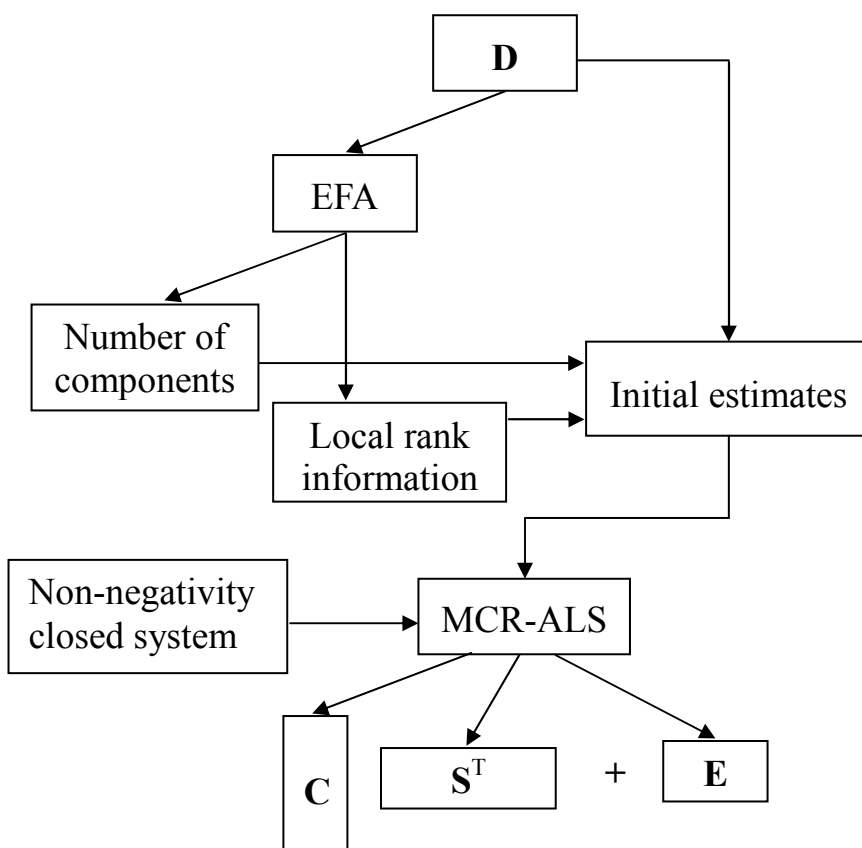
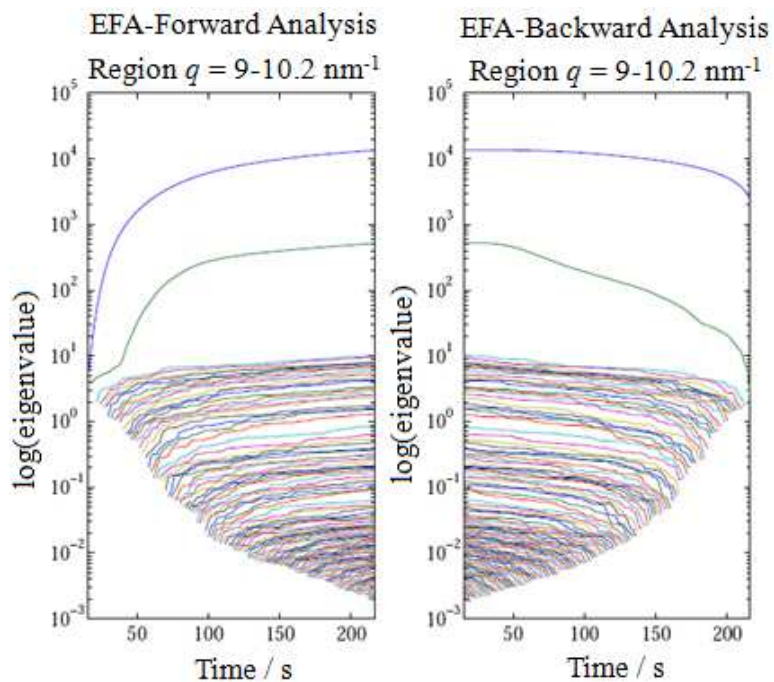**Figure S2-1:** The operating procedure of MCR-ALS technique.

Figure S2-2: Results of EFA forward and backward analysis of the experimental matrix of WAXD diffraction profiles ($q = 9 – 10.2$ nm^{-1}).
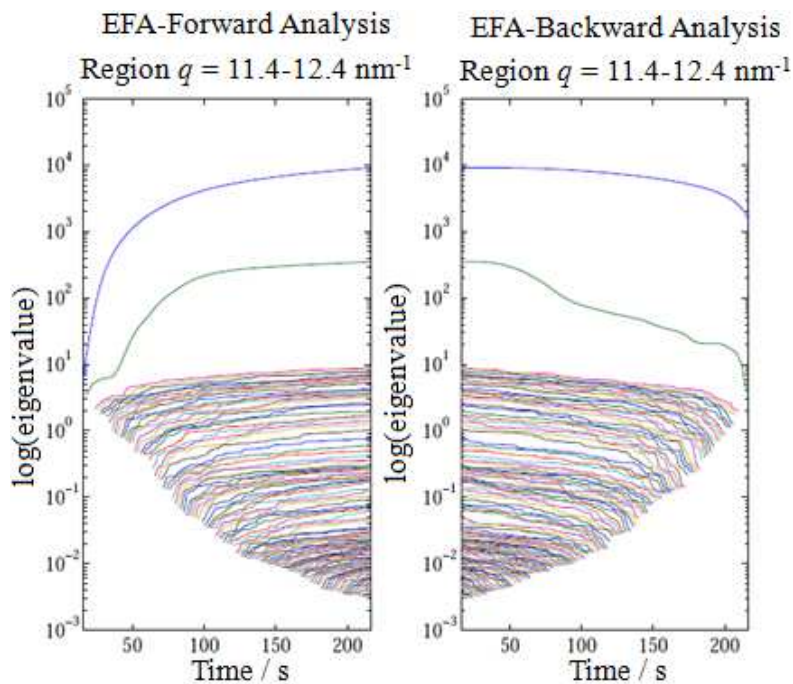

Figure S2-3: Results of EFA forward and backward analysis of the experimental matrix of WAXD diffraction profiles ($q = 11.4 – 12.4$ nm^{-1}).
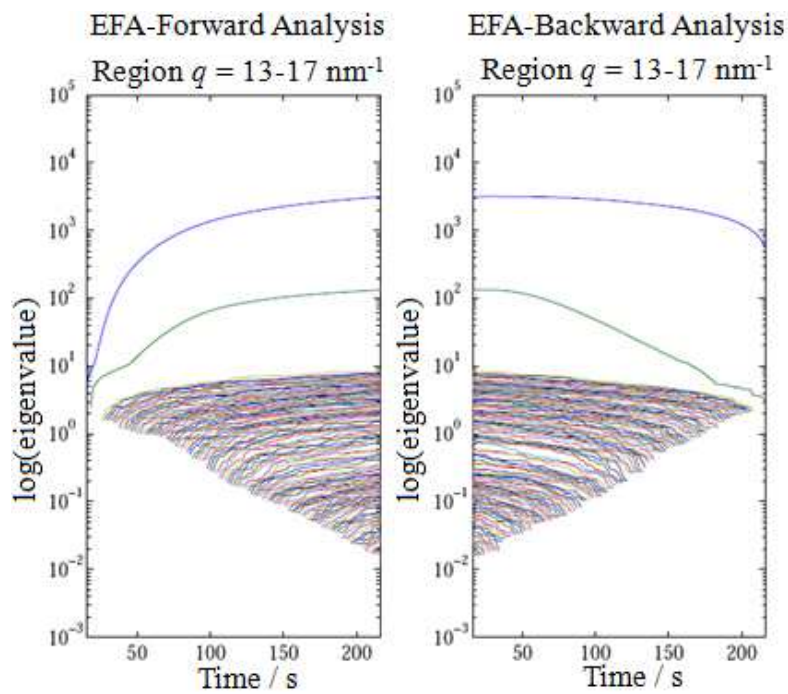
Figure S2-4: Results of EFA forward and backward analysis of the experimental matrix of WAXD diffraction profiles ($q = 13 – 17$ nm^{-1}).
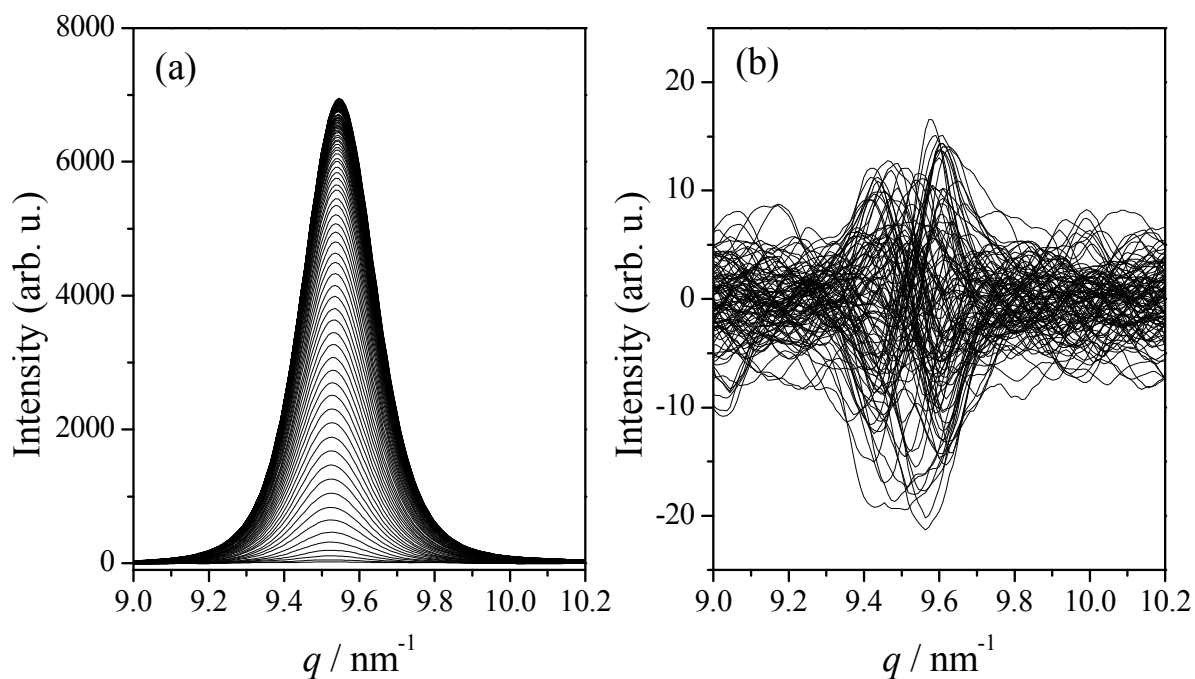

Figure S2-5: Experimental time-resolved WAXD diffraction profiles (a) and the residual matrix (b) through the MCR-ALS analysis in q region of $9 – 10.2$ nm^{-1}.
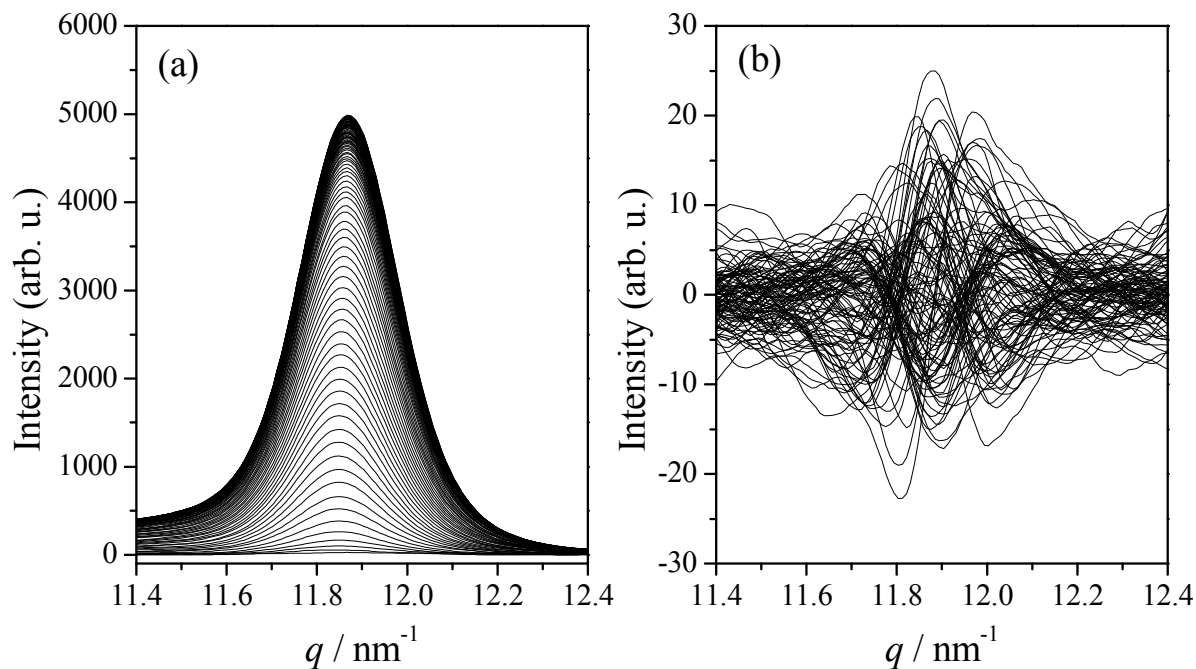
Figure S2-6: Experimental time-resolved WAXD diffraction profiles (a) and the residual matrix (b) through the MCR-ALS analysis in q region of $11.4 - 12.4$ nm^{-1}.
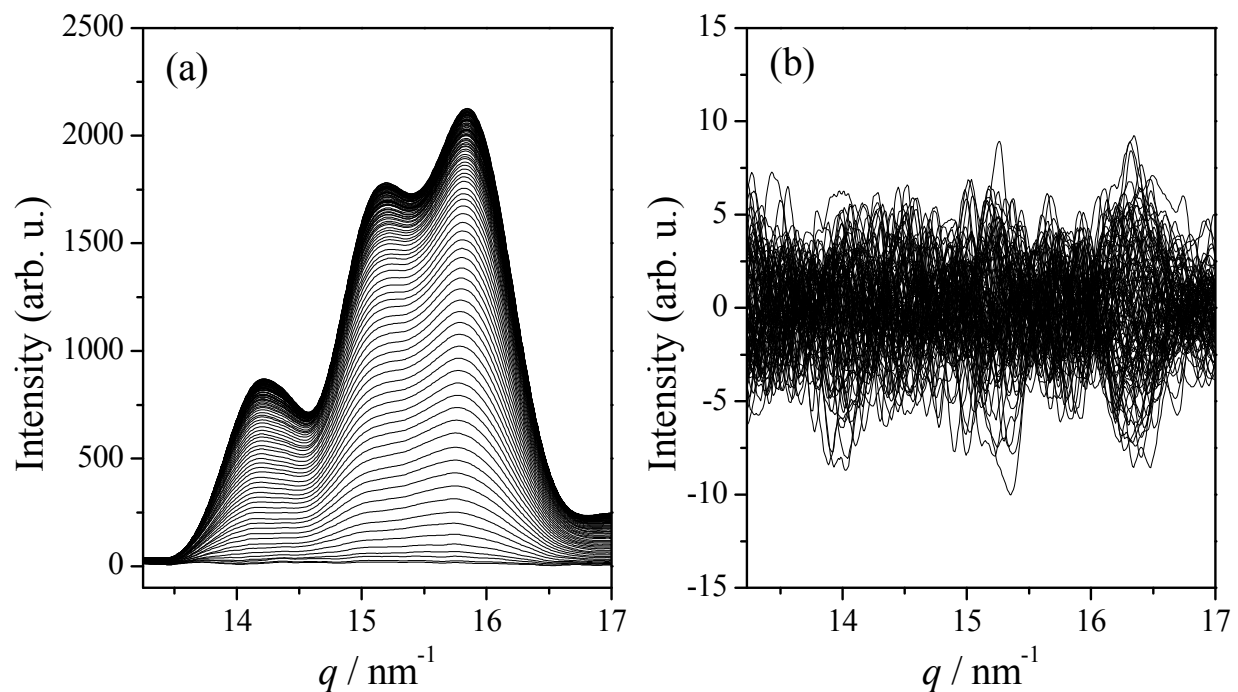

Figure S2-7: Experimental time-resolved WAXD diffraction profiles (a) and the residual matrix (b) through the MCR-ALS analysis in q region of $13 - 17$ nm^{-1}.

Supporting Information 3: Avrami Plots on $X_{C,app}(t)$ and $X_{crys}(t)$

The Avrami equation was applied to analyze the isothermal crystallization kinetics of PHB,

$$1 - X(t)/X(t = \infty) = \exp(-kt^n) \qquad (S3.1)$$

where $X(t)$ and $X(t=\infty)$ are the crystallinity at a given time t after the induction time and that at the long time limit, respectively, k is the crystallization rate constant, and n is the Avrami exponent. The apparent crystallinity $X_{C,app}(t)$, which includes both the intermediate structures and the lamellar crystallites, and the crystallinity $X_{crys}(t)$, which includes only the lamellar crystallites, were employed for $X(t)$ in eq 1. The Avrami plots of $\ln\{-\ln[1-X_{C,app}(t-t_0)/X_{C,app}(t = 218s)]\}$ vs $\ln(t-t_0)$ with $t_0 = 14$ s and $\ln\{-\ln[1-X_{crys}(t-t_I)/X_{crys}(t = 218s)]\}$ vs $\ln(t-t_I)$ with $t_I = 32$ s are shown in Figures S3-1 (a) and (b), respectively, where t_0 and t_I are the respective induction periods. From the slopes and intercepts of the straight lines in Figures S3-1 (a) and (b), the Avrami exponent n and the rate constant k can be determined: $n = 1.8$, and $k = 0.000825$ s$^{-1.8}$ for $X_{C,app}(t)$; $n = 1.5$, and $k = 0.00303$ s$^{-1.5}$ for $X_{crys}(t)$. Figures S3-1 (a) and (b) show the deviation from the linear-fitting at $t > 100$ s, seemingly due to onset of the secondary crystallization process.
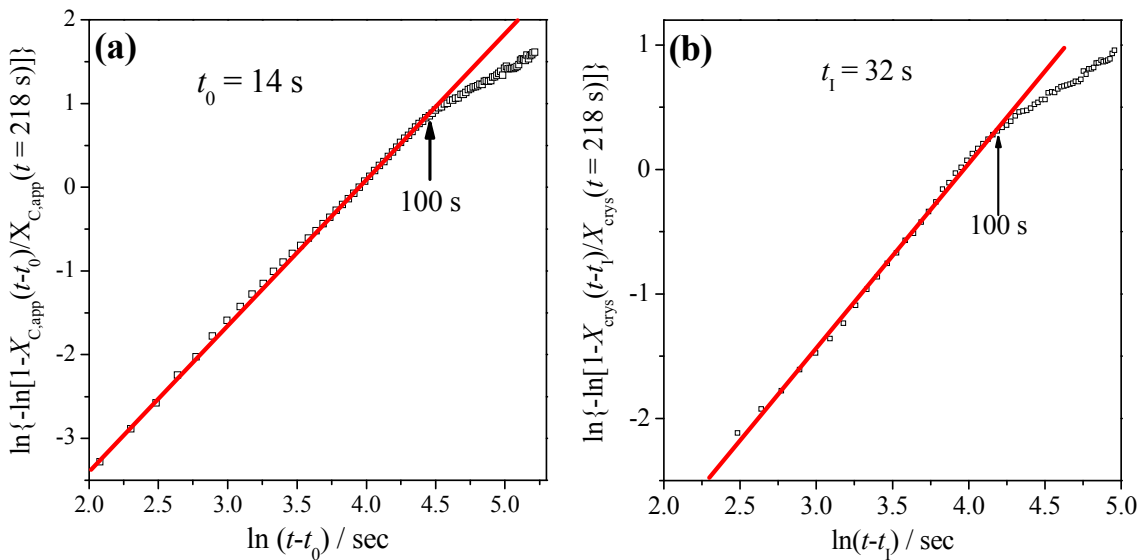

Figure S3-1: The Avrami Plots on $X_{C,app}(t)$ with $t_0 = 14$ s (part a) and $X_{crys}(t)$ with $t_I = 32$ s (part b).

Supporting Information 4: Heterospectral and Homospectral 2D-COS Analyses with tr-SAXS Profiles and Their Results

A very intriguing possibility found in the 2D correlation spectroscopy is the idea of *hetero-spectral* 2D correlation spectroscopy which conducts the 2D correlation analysis between two completely different types of spectra simultaneously measured for a given system under a given external perturbation.[10] In the present study, we employed the heterospectral 2D correlation analysis between the time-resolved WAXD (tr-WAXD) and Lorentz-corrected SAXS (tr-SAXS) profiles. We calculated the matrix $\widetilde{\mathbf{X}}$ which shows difference profiles between the tr-SAXS profiles or tr-WAXD profiles at given times and the time-averaged respective profiles,

$$\widetilde{\mathbf{X}} = \mathbf{X} - \overline{\mathbf{X}} \tag{S4.1}$$

where $\mathbf{X}$ is the experimentally obtained matrices of tr-SAXS and tr-WAXD profiles, and $\overline{\mathbf{X}}$ is the respective matrices on the time-averaged profiles. Subsequently, synchronous and asynchronous correlation intensities, defined as Φ and Ψ, respectively, can be obtained[10]:

$$\Phi = \frac{1}{n-1}\widetilde{\mathbf{X}}_{\mathrm{WAXD}}^{\mathrm{T}}\widetilde{\mathbf{X}}_{\mathrm{SAXS}}^{\mathrm{T}} \tag{S4.2}$$

$$\Psi = \frac{1}{n-1}\widetilde{\mathbf{X}}_{\mathrm{WAXD}}^{\mathrm{T}}\mathbf{N}\widetilde{\mathbf{X}}_{\mathrm{SAXS}}^{\mathrm{T}} \tag{S4.3}$$

where *n* is the number of profiles, and $\mathbf{N}$ is the Hilbert-Noda transformation matrix[10] defined as:

$$\mathbf{N} = \frac{1}{\pi}\begin{bmatrix} 0 & 1 & 2/1 & 3/1 & \dots \\ -1 & 0 & 1 & 2/1 & \dots \\ -2/1 & -1 & 0 & 1 & \dots \\ -3/1 & -2/1 & -1 & 0 & \dots \\ \dots & \dots & \dots & \dots & \dots \end{bmatrix} \tag{S4.4}$$

Here, $\widetilde{\mathbf{X}}_{\mathrm{WAXD}}^{\mathrm{T}}$ and $\widetilde{\mathbf{X}}_{\mathrm{SAXS}}^{\mathrm{T}}$ stand for the transpose matrices of $\widetilde{\mathbf{X}}_{\mathrm{SAXS}}$ and $\widetilde{\mathbf{X}}_{\mathrm{WAXD}}$, respectively.

One may worry about the effect of the peak shift with time in the tr-SAXS profiles as shown in Figure 3 on the rigorous evaluation of Φ and Ψ. We believe that the peak shift does not cause any problems on the evaluation of Φ and Ψ as long as the tr-SAXS profiles are obtained with accuracy and that it contains important physical meanings so that it cannot be artificially suppressed. Nevertheless, if necessary, one can obtain the 2D-COS with reduced tr-SAXS profiles which are plotted as a function of the reduced scattering vector q/q_{max} where q_{max} is the time-dependent q value at the scattering maximum, yielding $L(t) = 2\pi/q_{max}(t)$ as shown in Figure 12 in the text. The Lorentz-corrected reduced SAXS profiles with the reduced scattering vectors have a peak at $q/q_{max} = 1$, independent of time and thereby no peak-shift with time. Figure S4-1 shows the synchronous (part a) and asynchronous heterospectral 2D-COS (part b) between the tr-WAXD profiles and the Lorentz-corrected reduced tr-SAXS profiles, while Figure S4-2 shows the synchronous (part a) and asynchronous homospectral 2D-COS (part b) of the Lorentz-corrected reduced tr-SAXS profiles themselves, both taken from 16 to 32 s in time region I in the isothermal crystallization process. Figures S4-1 (a) and (b) are consistent with Figures 13 (a) and (b), respectively, while Figures S4-2 (a) and (b) are consistent with Figures 13 (c) and (d), respectively. Both results give the same conclusion as described in sections IV-7 and IV-8 in the text.
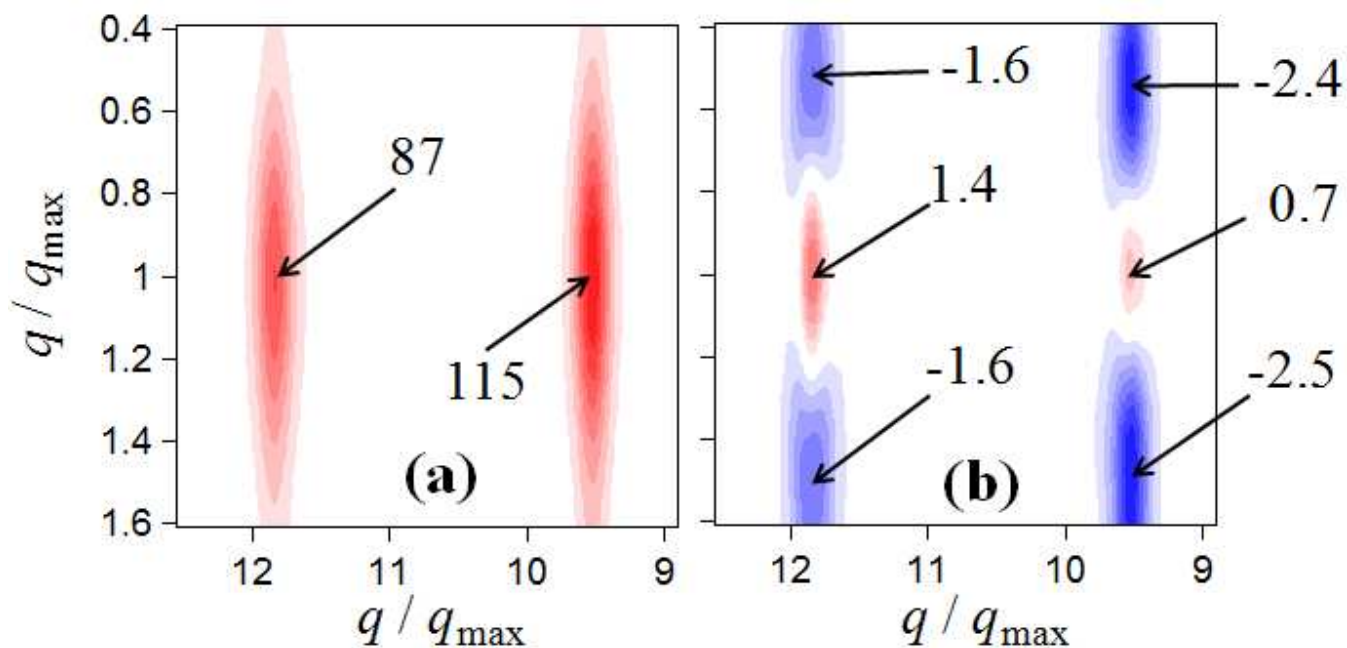
Figure S4-1: Synchronous (a) and asynchronous heterospectral 2D-COS (b) between the tr-WAXD profiles and the Lorentz-corrected reduced tr-SAXS profiles (in time region I) from 16 to 32 s. The numbers in the maps show the maximum intensity for the red positive part and the minimum intensity for the blue negative part.
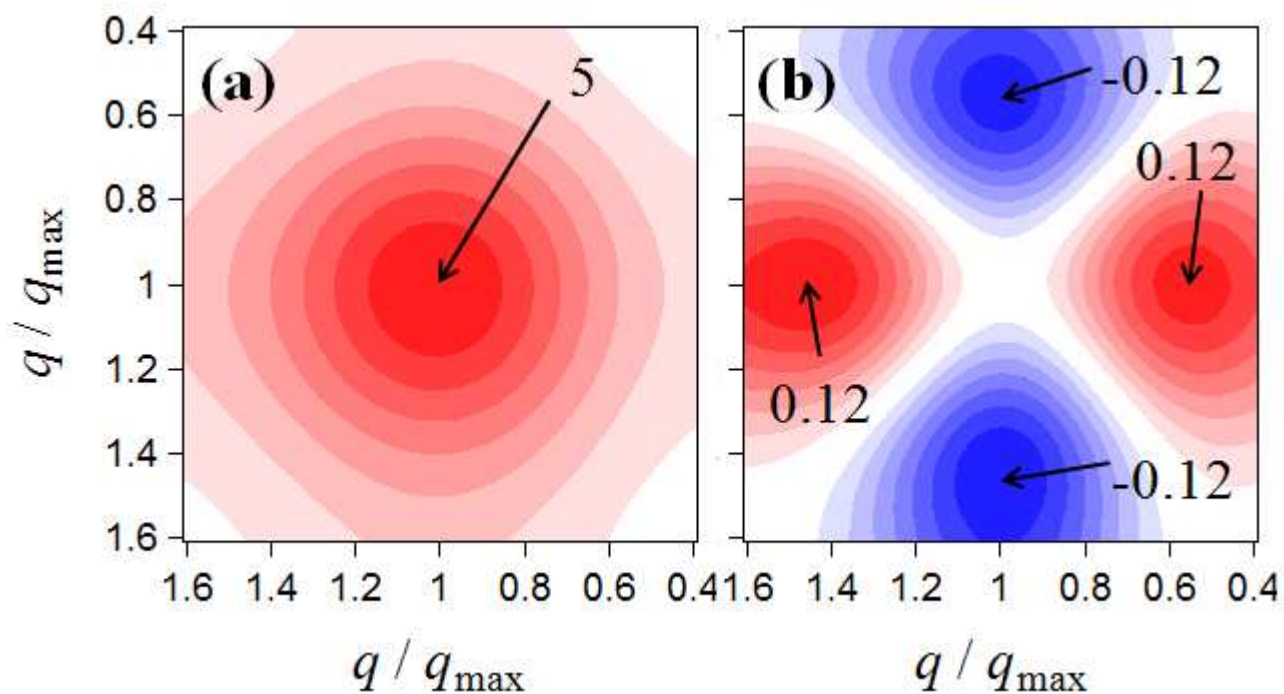

Figure S4-2: Synchronous (a) and asynchronous homospectral 2D-COS (b) between the Lorentz-corrected reduced tr-SAXS profiles themselves in time region I from 16 to 32 s.

Reference:

1. Strobl, G. R.; Schneider, M. *J. Polym. Sci.: Polym. Phys. Ed.* **1980,** *18*, 1343-1359.

2. Karjlainen, E. J. *Chemom. Intell. Lab. Syst.* **1989**, 7, 31-38.

3. Tauler, R.; Kowalski, B.; Fleming, S. *Anal. Chem.* **1993**, 65, 2040- 2047.

4. Tauler, R. *Chemom. Intell. Lab. Syst.* **1995**, 30, 133-146.

5. Tauler, R.; Smidile, A. K.; Kowalski, B. J. *Chemom.* **1995**, 9, 31-58.

6. Juan, D.; Tauler, R. *Anal. Chim. Acta* **2003**, 500, 195-210.

7. Maeder, M. *Anal. Chem.* **1987**, 59, 527-530.

8. Golub, G. H.; Loan, F. V. *Matrix Computations*, Johns Hopkins University Press: Baltimore, MD, **1983**.

9. *The Mathwork*, Natick, MA, MATLAB version **6.5. 2002**.

10. Noda, I.; Ozaki, Y. *Two-Dimensional Correlation Spectroscopy*; John Wiley & Sons: Chichester, UK. **2004**.